Available online at www.sciencedirect.com
ScienceDirect
Ceramics International 37 (2011) 393–398
CERAMICS INTERNATIONAL
www.elsevier.com/locate/ceramint

Short communication

Effects of annealing temperature on some structural and optical properties of ZnO nanoparticles prepared by a modified sol–gel combustion method

A. Khorsand Zak [a,b,*], M. Ebrahimizadeh Abrishami [b], W.H. Abd. Majid [a], Ramin Yousefi [c], S.M. Hosseini [b]

[a] Low Dimensional Material Research Center, Department of Physics, University of Malaya, Kuala Lumpur 50603, Malaysia
[b] Material and Electroceramics Lab., Department of Physics, Ferdowsi University of Mashhad, Mashhad 91775-1436, Iran
[c] Department of Physics, Islamic Azad University, Masjed-Soliman Branch, Masjed-Soliman, Iran

Received 10 April 2010; received in revised form 29 May 2010; accepted 14 July 2010
Available online 21 August 2010

Abstract

Plate-shaped zinc oxide nanoparticles (ZnO-NPs) were successfully synthesized by a modified sol–gel combustion method. Zinc acetate, pure water and isopropanol were used as the starting materials. Acetic acid, diethanolamine and nitric acid were used as the polymerization agent, complexing agent and fuel, respectively. The precursors were formed by mixing aqueous solutions of zinc acetate, acetic acid and diethanolamine. Nitric acid was used to dry the produced gel. The resulting xerogel was annealed at 600 °C, 650 °C and 750 °C for 1 h. The synthesized ZnO-NPs were characterized by X-ray diffraction analysis (XRD), thermogravimetric analysis (TGA) and high-magnification transmission electron microscopy (TEM). The XRD results revealed that the samples produced were crystalline with a hexagonal wurtzite phase. The TEM results showed single-crystal ZnO-NPs with nearly hexagonal plate shapes. The optical properties of the ZnO-NPs were studied by UV–visible and Fourier-transform infrared spectroscopy (FTIR). The UV–vis absorption spectra of the ZnO-NPs indicated absorption peaks in the UV region, which were attributed to the band gap of the ZnO-NPs. The results of the FTIR and UV–vis studies showed that the optical properties of the ZnO-NPs depended on the annealing temperature.

Keywords: A. Sol–gel processes; B. Combustion; C. X-ray diffraction; D. nanoparticles

1. Introduction

Zinc oxide (ZnO) exhibits several unique properties, such as semiconductivity and piezoelectric behavior [1], and it is consequently used in a wide variety of sensors and actuators. ZnO nanostructures have been explored for a wide range of applications in nanoscale devices, such as nanogenerators [2], sensors [3], field-emission transistors [4], ultraviolet photodetectors [5], and in biomedical systems, such as ultrasensitive DNA sequence detectors [6]. Apart from the technological significance of ZnO nanostructures, their quasi-one-dimensional structure, with diameters in the range of tens to hundreds of nanometers, makes them interesting from a scientific point of view. In this size range, they are expected to possess interesting physical properties and pronounced coupling quite different from their bulk counterpart [7].

Recently, several new routes have been developed for the synthesis of ZnO nanostructures, such as the organometallic precursor method [8], a microemulsion process [9], sol–gel synthesis [10], physical vapor deposition [11,12], precipitation [13], solvothermal and hydrothermal methods [14,15], and sol–gel combustion [16]. In the sol–gel combustion method, the raw materials, which are usually a nitrate compound and a fuel, are dissolved in water. After the pH is adjusted with a weak base such as ammonia, the mixed solution is then heated to convert the sol into a high-viscosity gel. Increasing the temperature of the gel causes an exothermic combustion process to occur. Annealing the resulting substance produces the final product [17]. Gel combustion gives homogenous, high-purity, and high-quality nanopowders with the possibility of stoichiometric

* Corresponding author at: Low Dimensional Material Research Center, Department of Physics, University of Malaya, Kuala Lumpur 50603, Malaysia. Tel.: +60 12 2850849.
E-mail address: alikhorsandzak@gmail.com (A.K. Zak).

0272-8842/$36.00
doi:10.1016/j.ceramint.2010.08.017

Table 1
The methods and solvents which used to prepare ZnO-NPs and their morphology.

Refs.	Method	Precursor material and solvents	Morphology
[10]	Sol–gel	Zinc nitrate, citric acid and distilled water	Whisker
[14]	Solvothermal	Zinc acetate, 1-butanol, 1-hexanol, 1-octanol and 1-decanol	Nanorod
[15]	Hydrothermal	Zinc acetate, cyclohexane, cetyltrimethyl ammonium bromide (CTAB), n-butylalcohol and distilled water	Hollow nanospheres and hexagonal microtubes
[25]	Solochemical	Zinc chloride, distilled water	Amorphous
[26]	Dehydration	Zinc acetate, alcohol	Spherical
Present work	Sol–gel combustion	Zinc acetate, citric acid and distilled water	Hexagonal nanoplate

control [18]. de Sousa et al. [19] used metallic nitrate with urea and made a ZnO nanopowders with a size of about 0.4–0.5 μm for a varistor application. Hwang and Wu [20] worked on ZnO nanopowder made by a combustion method. They used glycine as the fuel and metallic nitrates in a specific stoichiometric ratio. The morphology of the nanoparticles can be changed by changing the solvent; different morphologies give rise to different properties, as shown in Table 1.

In this study, a modified sol–gel combustion method was used to prepare ZnO nanoparticles, using nitric acid as the fuel, diethanolamine as the complexing agent and acetic acid as the polymerization agent. The size, morphology, crystallinity, and optical properties of the resulting ZnO particles were investigated as well as the influence of annealing temperatures on their size and optical properties.

2. Experimental

2.1. Preparation of ZnO-NPs

In order to prepare 10 g of the ZnO-NPs, 135 mL of pure water was mixed with 65 mL of isopropanol, and the solution was stirred for 5 min at 30 °C. Water is a necessary solvent to hydrolyze the solution, but disorder reactions can occur when adding excess water to the solution. The temperature was then increased to 45 °C, and 27 g of zinc acetate was gradually added to the solution. The stirring was continued to achieve a clear sol of Zn^{+} cations. In this process, suitable polymerization and complexing agents should be used. While citric acid and ethylene glycol are normally used for this application, in this work, acetic acid and diethanolamine were used as the polymerization and complexing agents, respectively. The high combustion temperature of citric acid, however, caused the reaction to be more difficult to control compared to the use of acetic acid. The weight ratio of these materials was chosen as follows:

(Diethanolamine/metal cation) = 1
(Acetic acid/metal cation) = 2

The acetic acid was mixed with diethanolamine, and the mixture was stirred to achieve a clear solution. Subsequently, the solution was added to the zinc solution. The mixture then stirred for 30 min at 40 °C. One of the advantages of using these materials is that the pH of the solution reaches 7 spontaneously without requiring the addition of ammonium hydroxide to control the pH. To obtain homogenous nanoparticles and a stable sol, the solution was then refluxed for 4 h at 110 °C (the refluxing temperature must be higher than the boiling temperature of the solvents). The solution was then placed in a water bath, and the temperature was held at 80 °C for 16 h to prepare a viscous gel from the refluxed sol. Finally, a xerogel was obtained by treating the gel with acid nitric. The xerogel was calcined for 2 h at 600 °C, 650 °C and 750 °C to obtain white ZnO-NP powders.

2.2. Characterization methods

The prepared ZnO-NPs were characterized by powder X-ray diffraction (XRD), ultraviolet–visible (UV–vis) spectroscopy, Fourier-transform infrared Spectroscopy (FTIR), thermogravimetry (TGA, Q600) and transmission electron microscopy (TEM). The phase evolutions and structure of the ZnO-NPs were studied by X-ray diffraction (Philips, X'pert, Cu Kα) and FTIR (ST-IR/ST-SIR spectrometer). The UV–vis spectra were recorded over the range of 350–700 nm with a Lambda 25-Perkin Elmer UV–vis spectrophotometer. Transmission electron microscopy (TEM) observations were carried out on a Hitachi H-7100 electron microscope. The band gap of the ZnO-NPs was calculated from the UV absorption results.

3. Results and discussion

3.1. TG and FTIR analyses

The TGA/DTA curves of ZnO-NPs synthesized by the sol–gel combustion method, as described in Section 2, are presented in Fig. 1. The TG traces show a minor weight loss (3%) during the heating step from 50 °C to 190 °C. This minor weight loss was attributed to the removal of physically absorbed water. A major weight loss (22%) was also observed in the step from 190 °C to 750 °C, which was related to the combustion of organic materials. No further weight loss was observed up to 900 °C. This indicates that the formation of ZnO nanocrystalline as the decomposition product was complete at 750 °C.

Fig. 2 shows the FTIR of the ZnO-NPs prepared by the sol–gel combustion method, in the range of 4000–280 cm^{-1}. A broad band is observed for each spectrum that is attributed to a Zn–O vibration mode. It is also observed that there is a negligible shift to a lower wavenumber due to increase in the annealing temperature. This shift can be related to a change in the lattice parameters of the ZnO-NPs. There were several

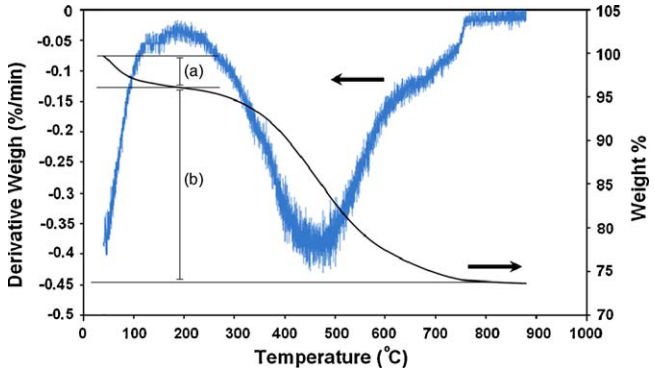

Fig. 1. TGA and DTA curves of xerogels from 50 °C to 900 °C. The traces show two steps; (a) is related to the evaporation of water and (b) is related to the decomposition of organic materials.

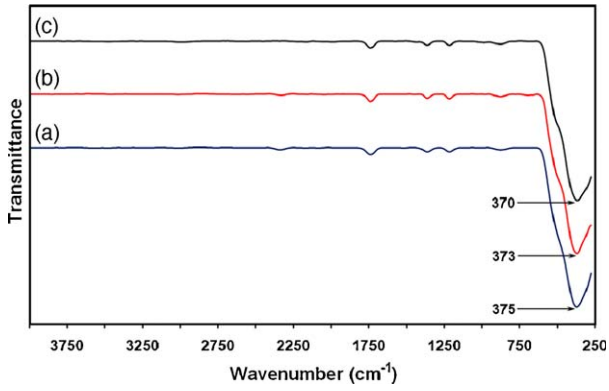

Fig. 2. FTIR spectra of the ZnO-NPs prepared at different annealing temperatures: (a) 600 °C, (b) 650 °C and (c) 750 °C. The absorption band related to Zn–O vibration mode was clearly observed.

absorption bands at 1750 cm^{-1}, 1350 cm^{-1} and 1250 cm^{-1}. These absorption bands were likely related to CO_2 absorbed from the atmosphere (air) and can therefore be neglected.

3.2. X-ray diffraction and particle-size analyses

The XRD patterns of the prepared samples are shown in Fig. 3. All the detectable peaks can be indexed to the ZnO wurtzite structure. The reflection peaks clearly became sharper with increasing thermal decomposition temperature, indicating an

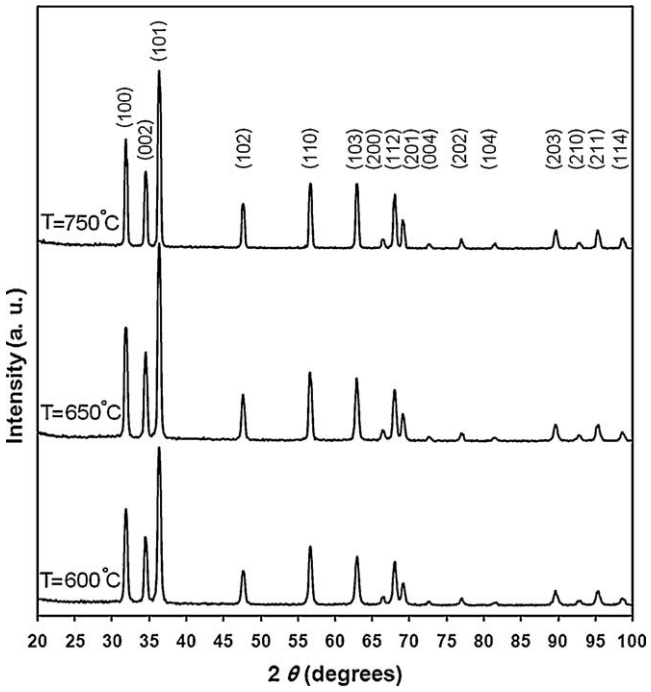

Fig. 3. XRD pattern of ZnO-NPs prepared at different annealing temperatures. A slight change of intensity and position was observed for the (2 0 1) peak.

enhancement of crystallinity. The wurtzite lattice parameters, e.g., the values of d, the distances between adjacent crystal planes ($h\ k\ l$), were calculated from the Bragg equation, $\lambda = 2d \sin\theta$; the lattice constants a, b and c, interplanar angles, the angles φ between the planes ($h_1\ k_1\ l_1$) of spacing d_1 and the plane ($h_2\ k_2\ l_2$) of spacing d_2 and the primary cell volumes were calculated from the Lattice Geometry equation [21]. It was observed that there was little change in the lattice parameters when the annealing temperature was increased. This change in lattice parameters can be attributed to the change of particle size and quantum size effects [22]. The lattice parameters of the ZnO-NPs calcined at different temperatures are summarized in Table 2.

Although TEM is the best way to determine the particle size of nanoparticles, XRD is also widely used. The Scherrer method for calculating particle size gives an average value. However, with TEM, besides directly measuring particle size, the morphology of the particles can also be observed. The crystal sizes of the ZnO-NPs were determined by means of an

Table 2
Lattice parameters of ZnO-NPs prepared at calcination temperatures of 600 °C, 650 °C and 750 °C (the measurements were done at room temperatures of 25 °C).

Temperature	$2\theta \pm 0.1$	$h\ k\ l$	$d_{h\ k\ l}$ (nm) $\pm$ 0.006	Structure	Lattice parameter (nm) $\pm$ 0.005 $\pm$ 0.01	V (nm^3) $\pm$ 0.2	Cos φ $\pm$ 0.002
600 °C	67.9 69.1	(1 1 2) (2 0 1)	0.138 0.136	Hexagonal	a = 0.322 c/a = 1.67	48.1	0.848
650 °C	67.9 69.0	(1 1 2) (2 0 1)	0.138 0.136	Hexagonal	a = 0.322 c/a = 1.66	48.0	0.848
750 °C	68.0 69.0	(1 1 2) (2 0 1)	0.138 0.136	Hexagonal	a = 0.322 c/a = 1.65	47.7	0.847

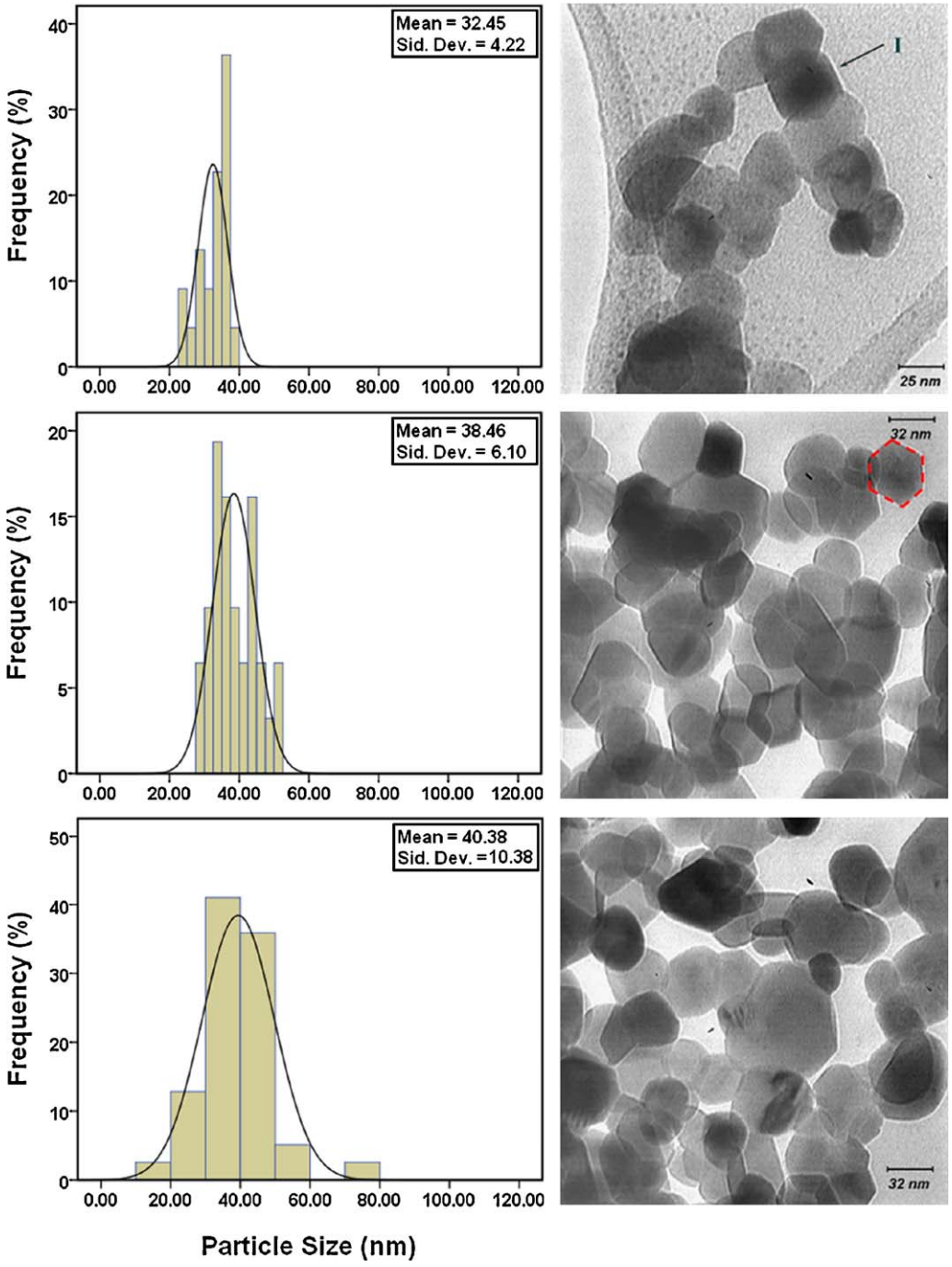

Fig. 4. TEM images of ZnO-NPs prepared at different annealing temperatures: (a) 600 °C, (b) 650 °C and (c) 750 °C. The nearly hexagonal plate shape of the ZnO-NPs is clearly shown (in I, for example).

X-ray line-broadening method using the Scherrer equation: $D = (k\lambda/\beta_{h\ k\ l} \cos\theta)$, where D is the particle size in nanometers, λ is the wavelength of the radiation (1.54056 Å for Cu Kα radiation), k is a constant equal to 0.94, $\beta_{h\ k\ l}$ is the peak width at half-maximum intensity and θ is the peak position. The (1 0 2) and (1 1 0) planes were chosen to calculate the crystal size (either plane can be used for this application); the results are presented in Table 3. The typical TEM result shows various hexagonal shapes with smooth surfaces. There was a ∼25% variation between the TEM and XRD results for particle size. In very small particles, the atoms on the surface apply a strain on the particle due to the surface effect [22], but we did not consider this effect in the XRD measurements. The TEM results are presented in Fig. 4.

3.3. UV–vis diffuse reflectance spectra

The UV–vis absorption spectra of the ZnO-NPs prepared at annealing temperatures of (a) 600 °C, (b) 650 °C and (c) 750 °C are shown in the inset of Fig. 5. The relevant increase in the

Table 3
The crystal size of ZnO-NPs prepared at calcination temperatures of 600 °C, 650 °C and 750 °C.

Temperature	$2\theta \pm 0.1$	FWHM ± 0.01	Average crystal size (nm)	
600 °C	47.5	0.53	17.1	18 ± 2
	56.6	0.50	19.0	
650 °C	47.5	0.49	18.4	19 ± 2
	56.6	0.50	19.0	
750 °C	47.5	0.44	20.8	21 ± 2
	56.6	0.44	21.4	

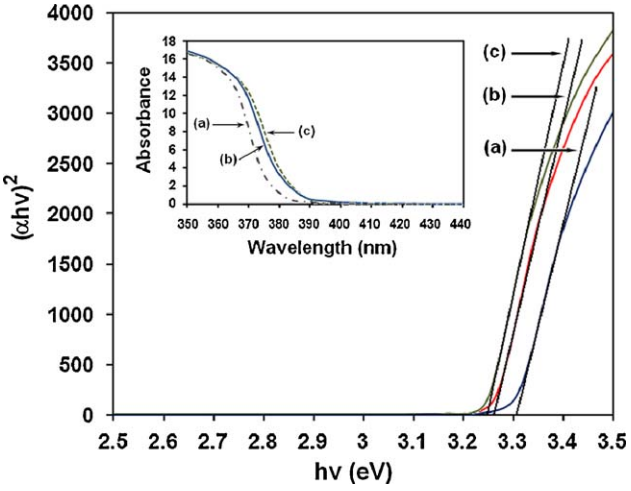

Fig. 5. Absorption edge (inset) and band gap of the ZnO-NPs prepared at different annealing temperatures: (a) 600 °C, (b) 650 °C and (c) 750 °C.

absorption at wavelengths less than 400 nm can be assigned to the intrinsic band-gap absorption of ZnO due to the electron transitions from the valence band to the conduction band ($O_{2p} \rightarrow Zn_{3d}$) [23]. Interestingly, an obvious redshift in the absorption edge was observed for the products annealed at different temperatures. This might be due to changes in their morphologies, particle size and surface microstructures. Moreover, the direct band-gap energies estimated from a plot of $(\alpha \times h\nu)^2$ versus the photo energy ($h\nu$) according to the Kubelka–Munk model [24], shown in Fig. 5, were 3.31 eV, 3.26 eV and 3.24 eV for the ZnO-NPs obtained at the increasing annealing temperatures of (a) 600 °C, (b) 650 °C and (c) 750 °C, respectively. Such an increase in the ZnO band-gap energy is in good agreement with the corresponding redshift seen in the absorption edge mentioned above.

4. Conclusions

A modified sol–gel combustion process was designed to prepare ZnO-NPs. The products were characterized by powder XRD, TGA, UV–vis and FTIR spectroscopy and TEM. The XRD results indicated the wurtzite structure of ZnO-NPs to be free from pyrochlore phase at annealing temperatures of 600 °C, 650 °C and 750 °C. Furthermore, the FTIR trace showed a broad absorption band related to Zn–O bond vibration. The calculated lattice parameters were observed to change with the annealing temperature. The change in the lattice parameters may be associated with particle size and quantum size effects. The size of the ZnO-NPs increased with an increase in annealing temperature. The band gap of the ZnO-NPs was estimated from the UV–vis absorption. It was observed that there was a redshift in the absorption edge at increased annealing temperature. From the TEM results, the average particle sizes of the ZnO-NPs annealed at the temperatures of 600 °C, 650 °C and 750 °C were determined to be 32 ± 4 nm, 38 ± 6 nm and 41 ± 9 nm, respectively, and the particles were nearly hexagonal in form.

Acknowledgment

This work was supported by University of Malaya through the Grant no. RG048/09AFR.

References

[1] A.V. Desai, M.A. Haque, Mechanical properties of ZnO nanowires, Sens. Actuators 134 (2007) 169–175.
[2] X. Wang, J. Song, Z.L. Wang, Nanowire and nanobelt arrays of zinc oxide from synthesis to properties and novel devices, J. Mater. Chem. 17 (2007) 711–720.
[3] N. Hongsith, C. Viriyaworasakul, P. Mangkorntong, N. Mangkorntong, S. Choopun, Ethanol sensor based on ZnO and Au-doped ZnO nanowires, Ceram. Int. 34 (2008) 823–826.
[4] M.S. Arnold, P. Avouris, Z.W. Pan, Z.L. Wang, Field-effect transistors based on single semiconducting oxide nanobelts, J. Phys. Chem. B 107 (2003) 659–663.
[5] J.H. Jun, H. Seong, K. Cho, B.M. Moon, S. Kim, Ultraviolet photodetectors based on ZnO nanoparticles, Ceram. Int. 35 (2009) 2797–2801.
[6] N. Kumar, A. Dorfman, J.I. Hahm, Ultrasensitive DNA sequence detection using nanoscale ZnO sensor arrays, Nanotechnology 17 (2006) 2875–2881.
[7] M. Law, J. Golldberger, P. Yang, semiconductor nanowires and nanotubes, Annu. Rev. Mater. Res. 34 (2004) 83–122.
[8] W. Chen, Y.H. Lu, M. Wang, L. Kroner, H.J. Fecht, Synthesis, thermal stability and properties of ZnO_2 nanoparticles, J. Phys. Chem. C 113 (2009) 1320–1324.
[9] P.Y. Wang, Q.H. Gao, J.Q. Xu, Study of photocatalytic activity of nanosized zinc peroxide, Fine Chem. 24 (2007) 436–440.
[10] H.Y. Yue, W.D. Fei, Z.J. Li, L.D. Wang, Sol–gel process of ZnO and $ZnAl_2O_4$ coated aluminum borate whiskers, J. Sol-Gel Sci. Technol. 44 (2007) 259–262.
[11] R. Yousefi, M.R. Muhamad, Effects of gold catalysts and thermal evaporation method modifications on the growth process of Zn1−xMgxO nanowires, J. Solid State Chem. 183 (2010) 1733–1739.
[12] R. Yousefi, B. Kamaluddin, The effects of annealing temperature on structural and optical properties of S-doped ZnO nanobelts, Solid State Sci. 12 (2010) 252–256.
[13] Q. Yang, W. Hu, A novel mercury-media route to synthesize ZnO hollow microspheres, Ceram. Int. 36 (2010) 989–993.
[14] P. Tonto, O. Mekasuwandumrong, S. Phatanasri, V. Pavarajarn, P. Praserthdam, Preparation of ZnO nanorod by solvothermal reaction of zinc acetate in various alcohols, Ceram. Int. 34 (2008) 57–62.
[15] J. Wang, N. Shi, Y. Qi, M. Liu, Reverse micelles template assisted fabrication of ZnO hollow nanospheres and hexagonal microtubes by a novel fast microemulsion-based hydrothermal method, J. Sol-Gel Sci. Technol. 53 (2009) 101–106.

[16] N. Riahi-Noori, R. Sarraf-Mamoory, P. Alizadeh, A. Mehdikhani, Synthesis of ZnO nano powder by a gel combustion method, J. Ceram. Process. Res. 9 (2008) 246–249.
[17] W.S. Chiu, P.S. Khiew, D. Isa, M. Clike, S. Radiman, R. Abd-Shuko, M.H. Abdullah, N.M. Huang, Synthesis of two-dimensional ZnO nanopellets by pyrilysis of zinc oleate, Chem. Eng. J. 142 (2008) 337–343.
[18] Z. Yue, L. Li, J. Zhou, H. Zhang, Z. Gui, Preparation and characterization of NiCuZn ferrite nanocrystalline powders by auto-combustion of nitrate–citrate gels, Mater. Sci. Eng. B 64 (1999) 68–72.
[19] V.C. de Sousa, M.R. Morelli, R.H.G. Kiminami, Combustion process in the synthesis of ZnO–Bi_2O_3, Ceram. Int. 26 (2000) 561–564.
[20] C.C. Hwang, T.Y. Wu, Synthesis and characterization of nanocrystalline ZnO powders by a novel combustion synthesis method, Mater. Sci. Eng. B 111 (2004) 197–206.
[21] B.D. Cullity, Elements of X-ray Diffraction: A Practical Approach, Addison-Wesley Publishing Company Inc., California, 1956.
[22] M. Hosokawa, K. Nogi, M. Naito, T. Yokoyama, Nanoparticle Technology Handbook, Elsevier, Amsterdam, 2007.
[23] H. Yu, J. Yu, B. Cheng, M. Zhou, Effects of hydrothermal post-treatment on microstructures and morphology of titanate nanoribbons, J. Solid State Chem. 179 (2006) 349–354.
[24] J. Yu, C. Li, S. Liu, Effect of PSS on morphology and optical properties of ZnO, J. Colloid Interface Sci. 326 (2008) 433–438.
[25] M.R. Vaezi, S.K. Sadrnezhaad, Nanopowder synthesis of zinc oxide via solochemical processing, Mater. Des. 28 (2007) 515–519.
[26] H.K. Yadav, V. Gupta, K. Sreenivas, S.P. Singh, B. Sundarakannan, R.S. Katiyar, Low frequency Raman scattering from acoystic phonons confined in ZnO nanoparticles, Phys. Rev. Lett. 97 (2006) 085502.